The Journal of Chemical Physics

RESEARCH ARTICLE | DECEMBER 01 2025

Density functional theory study of mesophase formation in model lipid systems FREE

Special Collection: Self-Assembly: From Blueprints to Breakthroughs

Sahire Azam Ansary ; Gianmarco Munaò ; Valeria Conti Nibali

J. Chem. Phys. 163, 215101 (2025)
https://doi.org/10.1063/5.0289910

AIP Publishing

The Journal of Chemical Physics ARTICLE pubs.aip.org/aip/jcp

Density functional theory study of mesophase formation in model lipid systems

Cite as: J. Chem. Phys. 163, 215101 (2025); doi: 10.1063/5.0289910
Submitted: 10 July 2025 • Accepted: 30 October 2025 •
Published Online: 1 December 2025

Sahire Azam Ansary, Gianmarco Munaò,[a] and Valeria Conti Nibali[a]

AFFILIATIONS

Department of Mathematical and Computer Sciences, Physical Sciences and Earth Sciences, University of Messina, 98166 Messina, Italy

Note: This paper is part of the Special Topic, Self-Assembly: From Blueprints to Breakthroughs.
[a]**Authors to whom correspondence should be addressed:** gianmarco.munao@unime.it and valeria.continibali1@unime.it

ABSTRACT

The emergence of mesophases in phospholipids is a fascinating phenomenon, which finds application in a wealth of research fields, from designing of building blocks to drug delivery. Here, we investigate structural properties and phase behavior of a coarse-grained model for phospholipid systems, represented by a dipolar Gay–Berne potential, within the framework of Percus–Yevick (PY) integral equation theory and classical density functional theory (DFT), with the aim of shedding light on the appearance of mesophases. Despite the well-known efficiency of PY theory in predicting structure, thermodynamics, and phase behavior of fluids at relatively low computational cost, we are not aware of any previous applications to phospholipid systems modeled through this potential. We focus on the role played by density, temperature, and dipolar head group strengths on the pair correlation functions of the phospholipid molecules, assessing our theoretical predictions against molecular dynamics simulations. Then, we utilize such correlation functions as structural input for DFT in order to locate the liquid crystalline phase transitions, with a particular emphasis on isotropic–nematic and nematic–smectic A transitions. The results highlight that enhanced dipolar interactions are able to stabilize ordered phases at low densities and high temperatures. This is indicated by the increase in orientational and translational order parameters and by the heightened compressibility in the smectic phase. Three different phase diagrams, corresponding to the different head group strengths investigated, are also drawn. A qualitative agreement with simulations is found, even though the densities at which transitions take place are typically underestimated.

I. INTRODUCTION

Lipids are essential components of living organisms, as they play a crucial role in various biological processes that occur in water environments and are ubiquitous in nature.[1] Most lipids are amphiphilic elongated molecules, with a head group comprising one or more water-attracting (hydrophilic) functional groups and one or two water-repelling (hydrophobic) fatty acid chains.[2] In this context, a wide interest is aroused by zwitterionic phospholipids, a specific class of lipids containing an equal number of positively and negatively charged functional groups that are recognized as key components of biomembranes.[3,4] The importance of these molecules is mainly due to their polar nature, which arises primarily from the charge separation between nitrogen and phosphorus atoms within the head group[5,6] and causes a permanent and quite substantial electric dipole moment, which is around 18 D.[7] When phospholipids self-assemble into single-component bilayer membranes, with their hydrophobic tails facing inward and their hydrophilic heads facing outward, the permanent dipoles in each leaflet are oriented in opposite directions, resulting in the lack of an overall permanent dipole of the membrane. The orientation of the head group dipoles is not uniformly distributed and strongly depends on external conditions (charged species,[8] hydration level, and hydrostatic pressure[9]). On average, the lipid dipoles are preferentially oriented at an angle $\theta \approx 78°–80°$ with respect to the bilayer normal,[10–12] with the hydrophilic head groups rotationally decoupled from the hydrophobic tails.[9] Furthermore, it is well known that the electric potential difference across a membrane caused by dipolar potentials is substantial, ranging from 100 to 400 mV.[13] This potential difference plays a crucial role in numerous biological processes, including, among others, ion transport and signal transduction.[14,15]

In addition to the well-known examples of bilayers, the amphiphilic nature of phospholipids allows them to self-assemble into a wide variety of complex lyotropic liquid crystalline mesophases. Lipid-based lyotropic liquid crystals (LC) are highly ordered self-assembled structures formed by amphiphilic lipids in aqueous environments.[16] These systems are distinguished by their unique properties, including a high internal surface area and tunable phase transitions. Such characteristics make lipid LC systems particularly relevant, lately inspiring a range of applications in drug delivery and nanotechnology.[17–19]

In general, the most commonly observed liquid crystalline phases in a system of elongated molecules are the nematic (N) and smectic (S) phases.[20–23] In the nematic phase, the particles exhibit full translational symmetry but they tend to orient on average along a common direction called the nematic director. The partial breakdown of translational invariance and the simultaneous breaking of rotational invariance introduce smectic phases, where molecules are essentially confined in layers. The smectic A phase differs from the general smectic phase by having molecules arranged in layers with their long axes perpendicular to the layers, whereas in other smectic phases (smectic C and smectic H), the molecular orientations may be tilted relative to the layers.

The structure of the smectic A phase is very similar to L_α or fluid lamellar phase found in phospholipids.[24] Smectic H is also very similar to the $L_{\beta'}$ phase or gel phase.[24] A paradigmatic case is the multilayered myelin sheath in nerves, which is one of the most organized biological structures: it has properties similar to smectic liquid crystals and its interactions can be mostly understood by studying these states.[25,26] In addition, other biomacromolecules (such as rod-like virus, nucleic acids, and proteins) and glycolipids can exhibit thermotropic liquid crystal phases including both nematic and smectic.[27–29] Other mesophases can also be formed, including lamellar phases, inverted/reverse hexagonal structures, columnar structures, and continuous cubic arrangements.[30–35] In addition, both phospholipids and glycolipids can form a variety of lyotropic and thermotropic mesophases under specific conditions: for instance, large monodomain bilayer arrays exhibiting smectic A ordering can be prepared from dipalmitoyl lecithin–water mixtures at low hydration.[36] In addition, glycolipids[37] are known to display thermotropic smectic, columnar, and cubic mesophases depending on hydration and molecular packing. Furthermore, lipids can undergo liquid–liquid phase separation (LLPS), a fascinating process wherein a uniform mixture of multiple components naturally divides into two separate liquid phases, each with different component concentrations. LLPS has gained increasing recognition in the late 20th century for its significance in various biological contexts.[38–41]

In light of the wide variety of structures and phase behaviors which phospholipids may originate, the development of suitable models to reproduce their complexity through theoretical and simulation approaches is highly desirable. In the literature, both all-atom[30,42] and coarse-grained (CG)[43–51] models have been used to investigate the phase behavior and formation of lipid mesophases. Even highly coarse models, such as those based on implicit-solvent representations,[46,47,52] have been successfully implemented.

The Gay–Berne (GB) interaction potential[53,54] is one of such CG models that treat the effect of anisotropic attractive interactions and short-range repulsive interactions in an explicit and computationally efficient manner to reproduce the energy of interaction between two linear-tetratomic molecules with the potential of the four-site Lennard-Jones (LJ) system.[54] In the realm of LCs, the GB potential has become a standard model for studying liquid crystalline phases, and it is extensively used to investigate phenomena such as phase transitions, defect dynamics, molecular alignment under external fields, and self-assembly through both computer simulations[55–61] and theoretical approaches.[62–65] The possibility of including dipolar interactions within the GB potential gives rise to the dipolar GB model potential. Among the applications of the latter to lipid-based systems, Ayton *et al.*[66] and Whitehead *et al.*[67] employed a GB ellipsoid to model the large-scale properties of lipid bilayers; Sun and Gezelter[68] observed ripple phases using model lipids, each made up of a dipolar lipid head group and an ellipsoidal tail; recently, Paul *et al.*[10] studied the structure–property relationship of lipid biomembranes. The dipolar GB model potential has been shown to effectively elucidate the phase diagram and structural properties of lipid systems, making it well-suited for investigating the phase behavior of phospholipids where liquid crystalline structures are expected. Thus, the present model captures not only the bilayer-forming capacity of phospholipids but also their broader polymorphic behavior, which is essential for understanding lipid self-organization beyond the most physiologically relevant lamellar state.

The CG representation of DPPC, a typical phospholipid molecule, by means of the dipolar GB potential is pictorially given in the top panel of Fig. 1. A schematic representation of a pair of interacting GB particles, along with details of model parameters, is depicted in bottom panels of Fig. 1: the anisotropic tail of the phospholipid molecule is represented as a prolate ellipsoid (in red) using a Gaussian overlap potential. The head group of the lipid molecule is modeled as a point dipole (in blue) located at a distance $d = \sigma_0$ from the center of mass of the molecule along its long axis, where σ_0 is the length of the minor axis of the ellipsoid.

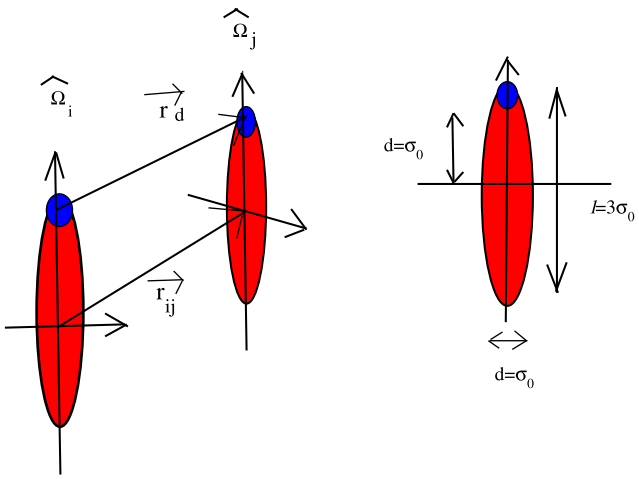

FIG. 1. Top panel: CG representation of a real lipid molecule (DPPC) based on the dipolar GB potential, in which the dipolar head group is depicted in blue and the non-polar ellipsoidal tail in red. Bottom panel: schematic representation of a pair of lipid molecules interacting via the GB dipolar potential (left) along with details of model parameters concerning a single lipid molecule (right).

Notably, all the studies on lipids using the GB model potential have been carried out by means of computer simulation techniques. The accuracy of simulations is influenced by factors such as the number of particles modeled and the simulation timescale, which can make achieving high precision computationally demanding. Conversely, different approaches such as integral equation theories of the fluid phase (IETs) operate in the thermodynamic limit and require considerably fewer computational resources. It is possible to investigate transitions among different phases using the classical density functional theory (DFT) approach, in which the required pair correlation functions are generally computed using the Percus–Yevick (PY) IET[69] over a grid of temperatures and densities. The reason of this choice is that IETs usually provide a reasonable description of the fluid structure,[70–73] while also being significantly efficient as well as Monte Carlo and molecular dynamics (MD) simulations.[74] In particular, PY is known to work reasonably well for systems with short range potentials (at the extreme, it offers analytical solution for a system of hard spheres). Since the GB potential successfully describes the short-range intermolecular forces for a wide variety of aspherical molecules, PY has been extensively used for these systems and found to produce correlations strong enough to stabilize isotropic, nematic, and smectic A phases, as well as to characterize mesophase stability and phase boundaries.[75–77] Moreover, PY offers a relatively simple analytical form for the pair correlation functions, which makes this specific IET minimally computationally demanding and straightforward to apply to complex systems such as the GB ellipsoidal model. In comparison with different, well known IETs, such as hypernetted-chain approximations (HNC), PY is known to be numerically stable and tractable for anisotropic fluids, whereas HNC often suffers from severe convergence difficulties in such systems and even loses solutions close to phase transitions.[78] However, to the best of our knowledge, no investigations employing PY have been conducted on phospholipid systems using this model potential so far.

In this paper, by implementing PY and the classical DFT of freezing,[79,80] we investigate structure, thermodynamics, and liquid crystalline phase behavior of phospholipids modeled by the dipolar GB potential.[56,57] We focus on the isotropic–nematic and nematic–smectic A phase transitions and determine the corresponding transition parameters. Thus, we explore open questions about the accuracy of DFT in modeling liquid crystalline transitions in phospholipids, the influence of pair correlation functions on transition parameters, and the effectiveness of the PY approach in accurately predicting structural and thermodynamic properties of such systems. Furthermore, considering that lipid phase transitions are markedly affected by the magnitude of the dipolar group, which varies among different lipids,[81] we have examined the extent to which variations in the dipolar moment influence the phase transition behavior. Finally, in order to substantiate our theoretical predictions, we have compared them with results from MD simulations, which we have carried out within the present study as well. In this context, it may be worth pointing out differences arising in comparison with previous studies of phospholipid models based on the GB potential, such as that presented in Ref. 10. In addition to the radically different computational approach (which, in our case, is prevalently based on PY and classical DFT rather than MD simulations), we also remark that while in Ref. 10 the authors implemented the GB potential to investigate the bilayer stability as a function of the lipid head group orientation, in our case the expansion in spherical harmonics requires an integration over the orientations of the ellipsoidal molecules, with the dipole moments fixed to the molecular axes. In addition, we focus on the role played by dipolar strength, which varies among different lipids, on the self-assembled mesophases.

This paper is organized as follows: in Sec. II, we discuss the details of the GB model potential with a dipolar head group of the phospholipid systems. This is followed in Sec. III by a brief discussion on the methodology concerning the PY approach along with its iterative solution method to calculate the pair correlation functions. Salient features of DFT suitable for the calculation of isotropic–nematic and nematic–smectic A transition parameters and an overview of MD simulations performed to validate theoretical predictions are also given in Sec. III. Our results are presented and discussed in Sec. IV, while conclusions follow in Sec. V. Finally, more technical details are presented in the Appendix.

II. MODEL POTENTIAL

The total intermolecular potential U_{Total} can be written as[10]

$$U_{\text{Total}} = U_{\text{GB}}(\hat{\mathbf{\Omega}}_i, \hat{\mathbf{\Omega}}_j, \hat{\mathbf{r}}_{ij}) + U_{\text{DD}}(\hat{\mathbf{\Omega}}_i, \hat{\mathbf{\Omega}}_j, \hat{\mathbf{r}}_d), \tag{1}$$

where U_{GB} denotes the GB potential, U_{DD} corresponds to the dipolar part of the potential, and $\hat{\mathbf{r}}_d$ is the distance between the two embedded point dipoles.

The first contribution is defined as[54]

$$U_{\text{GB}}(\hat{\mathbf{\Omega}}_i, \hat{\mathbf{\Omega}}_j, \mathbf{r}_{ij}) = 4\epsilon(\hat{\mathbf{\Omega}}_i, \hat{\mathbf{\Omega}}_j, \hat{\mathbf{r}}_{ij})\left[\left(\frac{r_{ij} - \sigma(\hat{\mathbf{\Omega}}_i, \hat{\mathbf{\Omega}}_j, \hat{\mathbf{r}}_{ij}) + \sigma_0}{\sigma_0}\right)^{-12} - \left(\frac{r_{ij} - \sigma(\hat{\mathbf{\Omega}}_i, \hat{\mathbf{\Omega}}_j, \hat{\mathbf{r}}_{ij}) + \sigma_0}{\sigma_0}\right)^{-6}\right], \tag{2}$$

where $\hat{\mathbf{r}}_{ij} = \mathbf{r}_{ij}/r_{ij}$ is a unit vector along the inter-molecular vector $\mathbf{r}_{ij} = \mathbf{r}_j - \mathbf{r}_i$ and unit vectors $\hat{\mathbf{\Omega}}_i$ and $\hat{\mathbf{\Omega}}_j$ represent the orientations of the ellipsoids. The shape anisotropy parameter $\sigma(\hat{\mathbf{\Omega}}_i, \hat{\mathbf{\Omega}}_j, \hat{\mathbf{r}}_{ij})$ and well depth anisotropy function $\epsilon(\hat{\mathbf{\Omega}}_i, \hat{\mathbf{\Omega}}_j, \hat{\mathbf{r}}_{ij})$ are defined as[54]

$$\sigma(\hat{\mathbf{\Omega}}_i, \hat{\mathbf{\Omega}}_j, \hat{\mathbf{r}}_{ij}) = \sigma_0\left[1 - \chi\left(\frac{(\hat{\mathbf{\Omega}}_i.\hat{\mathbf{r}}_{ij})^2 + (\hat{\mathbf{\Omega}}_j.\hat{\mathbf{r}}_{ij})^2 - 2\chi(\hat{\mathbf{\Omega}}_i.\hat{\mathbf{r}}_{ij})(\hat{\mathbf{\Omega}}_j.\hat{\mathbf{r}}_{ij})(\hat{\mathbf{\Omega}}_i.\hat{\mathbf{\Omega}}_j)}{1 - \chi^2(\hat{\mathbf{\Omega}}_i.\hat{\mathbf{\Omega}}_j)^2}\right)\right]^{-\frac{1}{2}} \tag{3}$$

and

$$\epsilon(\hat{\mathbf{\Omega}}_i, \hat{\mathbf{\Omega}}_j, \hat{\mathbf{r}}_{ij}) = \epsilon_0\epsilon_1^{\nu}(\hat{\mathbf{\Omega}}_i, \hat{\mathbf{\Omega}}_j)\epsilon_2^{\mu}(\hat{\mathbf{\Omega}}_i, \hat{\mathbf{\Omega}}_j, \hat{\mathbf{r}}_{ij}). \tag{4}$$

Here, the μ and ν exponents are adjustable parameters and ϵ_0 is the well depth of the cross-configuration of the particles, which is used to scale the energy. The two parameters μ and ν in the well depth function can take different sets of values without altering the relative well depths for the side-by-side and end-to-end configurations. σ_0 is the contact distance for the cross configuration of the ellipsoids. The functions $\epsilon_1(\hat{\mathbf{\Omega}}_\mathbf{i}, \hat{\mathbf{\Omega}}_\mathbf{j})$ and $\epsilon_2(\hat{\mathbf{\Omega}}_i, \hat{\mathbf{\Omega}}_j, \hat{\mathbf{r}}_{ij})$ are given by[54,73]

$$\epsilon_1(\hat{\mathbf{e}}_\mathbf{i}, \hat{\mathbf{e}}_\mathbf{j}) = \left[1 - \chi^2(\hat{\mathbf{\Omega}}_\mathbf{i}.\hat{\mathbf{\Omega}}_\mathbf{j})^2\right]^{-\frac{1}{2}}, \tag{5}$$

which favors the parallel alignments and

$$\epsilon_2(\hat{\mathbf{\Omega}}_i, \hat{\mathbf{\Omega}}_j, \hat{\mathbf{r}}_{ij}) = \left[1 - \chi'\left(\frac{(\hat{\mathbf{\Omega}}_i.\hat{\mathbf{r}}_{ij})^2 + (\hat{\mathbf{\Omega}}_j.\hat{\mathbf{r}}_{ij})^2 - 2\chi'(\hat{\mathbf{\Omega}}_i.\hat{\mathbf{r}}_{ij})(\hat{\mathbf{\Omega}}_j.\hat{\mathbf{r}}_{ij})(\hat{\mathbf{\Omega}}_i.\hat{\mathbf{\Omega}}_j)}{1 - \chi'^2(\hat{\mathbf{\Omega}}_i.\hat{\mathbf{\Omega}}_j)^2}\right)\right]. \quad (6)$$

The parameters χ and χ' measure the non-sphericity of the molecule and the energy anisotropy of the attractive forces between the GB ellipsoids, respectively. χ is a function of the length-to-breadth ratio $\kappa = l/d$ of the molecules, defined as

$$\chi = \frac{(l/d)^2 - 1}{(l/d)^2 + 1}. \quad (7)$$

The parameter χ' determines the energy anisotropy and it is defined as

$$\chi' = (1 - \kappa'^{1/\mu})/(1 + \kappa'^{1/\mu}), \quad (8)$$

where $\kappa' = \epsilon_{ee}/\epsilon_{ss}$ is the well-depth ratio between side-by-side (ϵ_{ee}) and end-to-end (ϵ_{ss}) configuration energy. Thus, the GB model includes four adjustable parameters: the aspect ratio κ (the ratio of the ellipsoid's semi-major to semi-minor axes), the energy anisotropy $\epsilon_{ee}/\epsilon_{ss}$, and the exponents μ and ν. While κ' measures the anisotropy of the repulsive core, it also defines the difference in the depth of the attractive well between the side-by-side and cross configurations. Both κ and κ' are crucial in stabilizing the liquid crystalline phases.

The behavior of potential energy curves for three particle orientations (side-by-side, T-shaped, and edge-to-edge) described by the GB potential is reported in Fig. 2: among the different orientations, the side-by-side geometry is the most favorable, as indicated by the deepest well depth.

The second term in Eq. (1), the potential U_{DD}, arises from dipole–dipole interactions between two particles,[69]

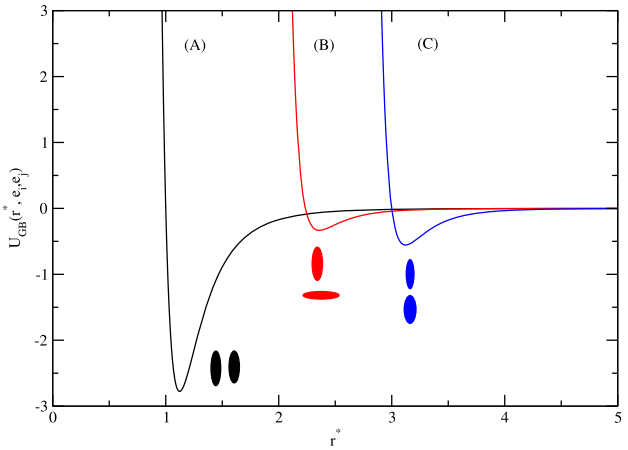

FIG. 2. Potential energy curves calculated using the GB potential for (A) the side-by-side (black), (B) the T-shaped (red), and (C) the edge-to-edge geometry (blue).

$$U_{DD}(\hat{\mathbf{\Omega}}_i, \hat{\mathbf{\Omega}}_j, \hat{\mathbf{r}}_d) = -\frac{q_i^* q_j^*}{r_d^3}[2c_i c_j - s_i s_j c'], \quad (9)$$

where $c_i = \cos\theta_i'$, $s_i = \sin\theta_i'$, and $c' = \cos(\phi_i - \phi_j)$, with θ_i' and ϕ_i' denoting the orientation of the dipole moment vector of molecule i. In particular, in the $\hat{r}_d$-frame, (θ_i', ϕ_i') and (θ_j', ϕ_j') define the orientations of the dipole moment vectors of molecules i and j, respectively. According to the schematic representation provided in Fig. 1, the point dipole (in blue) is located at a distance $d = \sigma_0$ from the center of mass of the molecule along its long axis, where σ_0 is the length of the minor axis of the ellipsoid. In our model, we consider the dipole moments aligned longitudinally along the long axis of the ellipsoids, following previous Monte Carlo simulations[53,82,83] and DFT[84] studies of dipolar GB potentials. Thus, the present model is thought as a first attempt to apply the GB ellipsoid framework to reproduce in a simplified way the onset of mesophases in phospholipids.

The quantities q_i^* and q_j^* represent the dipole moments of molecules i and j, respectively. In particular, $q^* = (\frac{q^2}{\epsilon_0 \sigma_0^3})^{\frac{1}{2}}$ is the dimensionless dipole moment of each molecule and r_d is the distance between point dipoles embedded on molecules i and j. In the present work, following a prescription reported in a previous study of GB model potential applied to lipid systems,[10] we set $\kappa = 3.0$, $\kappa' = 0.2$, $\mu = 1$, and $\nu = 2$. In addition, we consider three different values for the dipole moment q^*, specifically 0.5, 1.1, and 1.5, since it is known that in real lipid systems the dipole moment of the head group may change.[81,85] It is worth pointing out that these values, if converted to real units, are comparatively smaller than the dipole moment found in a real lipid molecule.[10] This actually compensates for not considering any explicit solvent interaction.

The GB potential parameters, such as anisotropy ratio and dipole moment, were specifically selected to reproduce the physical characteristics of lipid molecules under CG modeling. These parameters, including the angle of dipole moments and their orientation relative to the molecular axis, were validated by prior studies demonstrating their influence on phase transitions in lipid assemblies.[56] Such careful selection ensures our CG representation effectively captures the structural and dynamic rearrangements of lipid bilayers, providing a robust framework for understanding dipolar interactions and their physiological implications.

III. METHODS

A. The integral equation theory framework

The pair correlation function $g(\mathbf{x}_1, \mathbf{x}_2)$ plays a crucial role in the theory of molecular fluids and is strictly connected to the total correlation function, defined as $h(\mathbf{x}_1, \mathbf{x}_2) = g(\mathbf{x}_1, \mathbf{x}_2) - 1$.[70] Pair correlation functions are the lowest-order microscopic quantities that provide insight into the fluid structure and directly reflect the underlying intermolecular interactions. For a system of N particles confined within a volume V at a fixed temperature T, the pair correlation function is defined as follows:[70]

$$g_N(x_1, x_2) = \frac{\rho_N^{(2)}(x_1, x_2)}{\rho_N^{(1)}(x_1)\rho_N^{(1)}(x_2)}, \quad (10)$$

where $\rho_N^{(1)}(x_1)$ and $\rho_N^{(1)}(x_2)$ are the single-particle density distribution functions and $\rho_N^{(2)}(x_1, x_2)$ represents the pair density,

respectively. Here, $\mathbf{x} = (\mathbf{r}, \mathbf{\Omega})$ denotes both the position $\mathbf{r}$ of the molecule's center of mass and its orientation $\mathbf{\Omega}$, which is expressed in terms of Euler angles. For non-linear molecules, $\mathbf{\Omega}_i = (\alpha_i, \beta_i, \gamma_i)$; for linear molecules, $\mathbf{\Omega}_i = (\Theta_i, \Phi_i)$, with polar angles referring to an arbitrary space-fixed coordinate frame. The n-particle density $\rho_N^{(n)}(x_n)\, dx_n$ defines the probability of finding n particles in the system within the volume element $[dx_n = (d\mathbf{r}_n d\mathbf{\Omega}_n)]$, independently on the positions and orientations of other particles. Through particle densities, the pair correlation functions provide a complete description of the fluid structure at equilibrium. The structural information of an isotropic fluid is contained in the pair density distribution $\rho_N^{(2)}(x_1, x_2)$, as the single-particle density distribution is constant and equal to the overall number density, $\rho_N^{(1)}(x_i) = \rho_N^{(1)}(\mathbf{r}_i, \mathbf{\Omega}_i) = \rho_f = \langle N \rangle / V$. Thus, ρ_f corresponds to the fluid density. Due to the homogeneity (continuous translational symmetry) and isotropy (continuous rotational symmetry) of the system, pair functions such as $g^{(2)}(x_1, x_2)$ and $\rho^{(2)}(x_1, x_2)$ in the isotropic fluid depend solely on the interparticle distance $|\mathbf{r}_2 - \mathbf{r}_1| = r_{12}$, the relative orientation of the molecules, and the direction of r_{12}, which is represented by the unit vector $\hat{\mathbf{r}}_{12} = \frac{\mathbf{r}_{12}}{|r_{12}|}$. Therefore, for an isotropic fluid, Eq. (10) can be written as

$$\rho_f^2\, g_N(\mathbf{r}_{12}, \mathbf{\Omega}_1, \mathbf{\Omega}_2) = \rho_N(\mathbf{r}_{12}, \mathbf{\Omega}_1, \mathbf{\Omega}_2). \tag{11}$$

It follows that the pair structure of a fluid is completely determined by knowledge of $g_N(\mathbf{r}_{12}, \mathbf{\Omega}_1, \mathbf{\Omega}_2)$. The latter can be calculated as a function of intermolecular separation and orientation at a given temperature and density by solving the well-known Ornstein–Zernike (OZ) equation,[70]

$$h^{(2)}(\mathbf{r}_{12}, \mathbf{\Omega}_1, \mathbf{\Omega}_2) = c^{(2)}(\mathbf{r}_{12}, \mathbf{\Omega}_1, \mathbf{\Omega}_2) + \rho_f \int d\mathbf{3}\, c^{(2)}(\mathbf{r}_{13}, \mathbf{\Omega}_1, \mathbf{\Omega}_3) \times h^{(2)}(\mathbf{r}_{32}, \mathbf{\Omega}_3, \mathbf{\Omega}_2), \tag{12}$$

where $h^{(2)}(r_{12},\ \Omega_1,\ \Omega_2)$ and $c^{(2)}(r_{12},\ \Omega_1,\ \Omega_2)$ represent the total and direct pair correlation functions, respectively, while $d\mathbf{3} = d\mathbf{r}_3 d\mathbf{\Omega}_3$. Since the OZ equation links two unknown quantities, $h^{(2)}$ and $c^{(2)}$, an additional relation between them is needed to enable a solution. This relation is known as a closure relation. In the literature, several closure relations are available, such as PY, HNC, and modified hypernetted chain approximation (MHNC);[69] however, as stated in Sec. I, the implementation of closures other than PY is challenging in this case due to mathematical complexity of expanding them into spherical harmonics, as will be detailed afterward. Thus, in the present study, we chose the PY closure, expressed as

$$c^{(2)}(\mathbf{r}_{12}, \mathbf{\Omega}_1, \mathbf{\Omega}_2) = f(\mathbf{r}_{12}, \mathbf{\Omega}_1, \mathbf{\Omega}_2)\Big[g^{(2)}(\mathbf{r}_{12}, \mathbf{\Omega}_1, \mathbf{\Omega}_2) - c^{(2)}(\mathbf{r}_{12}, \mathbf{\Omega}_1, \mathbf{\Omega}_2)\Big], \tag{13}$$

in which $f(\mathbf{r}_{12}, \mathbf{\Omega}_1, \mathbf{\Omega}_2)$ is the Mayer function, defined as

$$f(r_{12}, \Omega_1, \Omega_2) = \exp\left[-\beta U_{Total}(r_{12}, \Omega_1, \Omega_2)\right] - 1, \tag{14}$$

with $\beta = (k_B T)^{-1}$. The interaction potential enters the equations through the closure relation. Together, the OZ equation and the closure relation form the IET, named according to the closure used. This theory provides a reliable and widely accepted approach to determine the equilibrium properties of homogeneous fluids. More technical details concerning the expansion of PY into spherical harmonics are presented in the Appendix.

B. Classical density functional theory of freezing

Classical DFT is a statistical mechanics approach to describe the thermodynamic properties of both ordered solids and fluids. It is a liquid-based approach, which regards the ordered phase as a strongly inhomogeneous fluid with frozen-in density modes. Classical DFT assumes the existence of a grand thermodynamic potential, $W(T,\ \mu_{chem}, [\rho])$, which is a functional of density and attains its minimum at the equilibrium density $\rho_{\mathrm{eq}}(x)$. Here, μ_{chem} denotes the chemical potential and $\mathbf{x} \equiv (\mathbf{r}, \mathbf{\Omega})$. The grand thermodynamic potential W is written as[79]

$$W = \beta \mathcal{A} - \beta \mu_{chem} \int d\mathbf{x} \rho(\mathbf{x}). \tag{15}$$

Here, $\mathcal{A}$ denotes the Helmholtz free energy, and $\rho(\mathbf{x})$ is a singlet distribution function. In the absence of an external potential, $\mathcal{A}$ can be expressed as

$$\mathcal{A}[\rho] = \mathcal{A}_{\mathrm{id}}[\rho] + \mathcal{A}_{\mathrm{ex}}[\rho_f], \tag{16}$$

where $\mathcal{A}_{\mathrm{id}}$ is the ideal free energy arising solely from the particles' kinetic energy and $\mathcal{A}_{\mathrm{ex}}$ represents the free energy contribution due to interparticle interactions. The kinetic energy component of the free energy is precisely known as[70]

$$\mathcal{A}_{\mathrm{id}}[\rho] = \int d\mathbf{x} \rho(\mathbf{x})[\log \rho(\mathbf{x}) \zeta^D - 1], \tag{17}$$

where D is the space dimension and $\zeta = h(\beta/2m\pi)^{1/2}$ is the thermal de Broglie wavelength. The excess part is expressed in terms of the direct pair correlation of the ordered phase $c^{(2)}[\mathbf{x}_1, \mathbf{x}_2;\ \rho]$ at its average density ρ as follows:

$$\frac{\delta^2 \mathcal{A}_{\mathrm{ex}}[\rho]}{\delta\rho(\mathbf{x}_1)\, \delta\rho(\mathbf{x}_2)} = -c^{(2)}[\mathbf{x}_1, \mathbf{x}_2; \rho]. \tag{18}$$

Since pair correlation functions of the ordered phase are generally not known, various approximations have been proposed, leading to different versions of DFT. We have used the well-known Ramakrishnan–Youssoff (RY) DFT,[80] in which the ordered phase correlation function is approximated by the correlation function of the coexisting isotropic liquid of the same chemical potential at the given temperature. Therefore, using the definition $\mathbf{x} \equiv (\mathbf{r}, \mathbf{\Omega})$, $\mathcal{A}_{ex}$ in the RY DFT can be obtained through a functional integration of Eq. (18) as

$$\mathcal{A}_{ex}[\rho] = \mathcal{A}[\rho_f] - \frac{1}{2} \int d\mathbf{r}_1 d\mathbf{\Omega}_1 \int d\mathbf{r}_2 d\mathbf{\Omega}_2\, \Delta\rho(\mathbf{r}_1, \mathbf{\Omega}_1) \times \Delta\rho(\mathbf{r}_2, \mathbf{\Omega}_2)\, c(\mathbf{r}_{12}, \mathbf{\Omega}_1, \mathbf{\Omega}_2; \rho_f), \tag{19}$$

where $\Delta\rho(\mathbf{r}_i,\mathbf{\Omega}_i) = \rho(\mathbf{r}_i,\mathbf{\Omega}_i) - \rho_f$, ρ_f is the density of the coexisting fluid, and $c(r_{12},\ \Omega_1,\ \Omega_2;\ \rho_f)$ is the direct correlation function of the isotropic fluid obtained from the IET. Substituting Eqs. (16)–(18) in Eq. (15), we obtain

$$\Delta W = \int d\mathbf{r}d\mathbf{\Omega}\left\{\rho(\mathbf{r},\mathbf{\Omega})\ln\left[\frac{\rho(\mathbf{r},\mathbf{\Omega})}{\rho_f}\right] - \Delta\rho(\mathbf{r},\mathbf{\Omega})\right\} - \frac{1}{2}\int d\mathbf{r}_1 d\mathbf{\Omega}_1 d\mathbf{r}_2 d\mathbf{\Omega}_2 \Delta\rho(\mathbf{r}_1,\mathbf{\Omega}_1) \times c(\mathbf{r}_{12},\mathbf{\Omega}_1,\mathbf{\Omega}_2;\rho_f)\Delta\rho(\mathbf{r}_2,\mathbf{\Omega}_2). \quad (20)$$

The ordered-phase density is obtained by minimizing ΔW with respect to arbitrary variations in the ordered-phase density, subject to the constraint that the orientational distribution is normalized to unity. This leads to the corresponding order parameter equation,[65,79]

$$\ln\frac{\rho(\mathbf{r}_1,\mathbf{\Omega}_1)}{\rho_f} = \lambda_L + \int d\mathbf{r}_2 d\mathbf{\Omega}_2 c(\mathbf{r}_{12},\mathbf{\Omega}_1,\mathbf{\Omega}_2;\rho_f)\Delta\rho(\mathbf{r}_2,\mathbf{\Omega}_2), \quad (21)$$

where λ_L is a Lagrange multiplier. Equation (21) is known as the order-parameter equation. To determine the freezing transition, we solve Eq. (21) to obtain $\rho(\mathbf{r}_1,\mathbf{\Omega}_1)$ with the symmetry of the ordered phase. Below a certain liquid density, the only solution is the uniform liquid $\rho(\mathbf{r},\mathbf{\Omega}) = \rho_f$; above this density, a spatially varying solution corresponding to the ordered phase emerges. To solve Eq. (21), the singlet distribution $\rho(\mathbf{r},\mathbf{\Omega})$ is parameterized as follows:

$$\rho(\mathbf{r},\Omega) = \rho_0\sum_q \sum_{l(even)} Q_{lq} e^{i\mathbf{G}_q\cdot\mathbf{r}} P_l(\cos\theta). \quad (22)$$

In the calculations, the sums are truncated at $l_{\max} = 4$ (even l only; we retain $l = 2, 4$) and at the fundamental layering mode, $q_{\max} = 1$; higher l and q harmonics are neglected. In addition, we set

$$Q_{lq} = \frac{2l+1}{N}\int d\mathbf{r}\int d\mathbf{\Omega}\rho(\mathbf{r},\mathbf{\Omega})e^{i\mathbf{G}_q\cdot\mathbf{r}} P_l(\cos\theta), \quad (23)$$

where $P_l(\cos\theta)$ is the Legendre polynomial of degree l and θ is the angle between the cylindrical axis of a molecule and the director. For the smectic A phase, we assume a one-dimensional periodic lattice along the z axis, consistent with $D_{\infty h}\times T(2)$ symmetry. In the smectic A phase, the continuous translational symmetry of the isotropic or nematic phase is broken along one direction, the layer normal (denoted as the z axis), leading to a periodic density modulation in that direction, while translational symmetry within the xy-plane remains preserved.[76] It is important to note that here the z axis does not refer to the laboratory space-fixed frame (SF), but rather to the director axis, i.e., the average orientation of the long molecular axes, which also coincides with the normal to the smectic layers. Accordingly, the reciprocal lattice vectors (taken as $\mathbf{G_q} = \frac{2\pi q}{d}\hat{z}$, where q is an integer index and d is the average interlayer spacing) are defined with respect to this axis.[79] On the other hand, in the nematic phase, which is translationally invariant, we need just the orientational singlet distribution function to determine the complete single particle distribution. To characterize the nematic phase, the orientational order parameters P_2 and P_4 are required, whereas for the smectic A phase, the translational order parameter along the z axis is needed.[75–77,79]

To quantify the degree of order in the system, we have considered two orientational order parameters, namely,

$$\bar{P}_l = \frac{Q_{l0}}{2l+1} = \langle P_l(\cos\theta)\rangle, \quad (24)$$

with l taking the values 2 or 4. The orientational order parameters are zero in the isotropic phase and nonzero in the liquid crystal phases, becoming equal to one in the limit of the complete orientational order. In addition, we consider one order parameter corresponding to the positional order along the z axis, namely,

$$\Lambda = Q_{00}(G_z) = \left\langle\cos\left(\frac{2\pi z}{d}\right)\right\rangle, \quad (25)$$

where $G_z = \mathbf{G_q}\cdot\hat{z}$ denotes the component parallel to the layer normal and $Q_{00}(G_z)$ is the positional order parameter that measures the first harmonic of density modulation along the z axis, with d being the inter-layer spacing of the smectic phase. Accordingly, this order parameter is nonzero in the smectic phase and disappears in isotropic and nematic phases. Finally, we also have one mixed-order parameter defined as

$$\tau = \frac{1}{5}Q_{20}(G_z) = \left\langle\cos\left(\frac{2\pi z}{d}\right)P_2(\cos\theta)\right\rangle. \quad (26)$$

The angular bracket in the above-mentioned equations indicates the ensemble average.

Upon substituting Eqs. (24)–(26) in Eq. (23), we obtain the following order parameters:

$$\bar{P}_l = \frac{1}{2d}\int_0^d dz\int_0^\pi \sin\theta d\theta P_l(\cos\theta)\exp(I), \quad (27)$$

$$\Lambda = \frac{1}{2d}\int_0^d dz\int_0^\pi \sin\theta d\theta\cos\left(\frac{2\pi z}{d}\right)\exp(I), \quad (28)$$

$$\tau = \frac{1}{2d}\int_0^d dz\int_0^\pi \sin\theta\, d\theta\cos\left(\frac{2\pi z}{d}\right)P_2(\cos\theta)\exp(I). \quad (29)$$

The change in density between ordered phase and isotropic fluid phase at the transition is given as

$$\triangle\rho^* = \frac{1}{2d}\int_0^d dz\int_0^\pi \sin\theta d\theta\exp(I) - 1. \quad (30)$$

Here, $\Delta\rho^* = \frac{\rho_o^* - \rho_f^*}{\rho_f^*}$ is the change in the density at the transition, where ρ_o^* and ρ_f^* are the average number densities of the particles in the ordered phase and the fluid phase, respectively,

$$I = \triangle\rho^*\hat{C}_{00}^0 + 2\Lambda\cos\left(\frac{2\pi z}{d}\right)\hat{C}_{00}^1(\theta) + \bar{P}_2\hat{C}_{20}^0(\theta) + \bar{P}_4\hat{C}_{40}^0(\theta) + 2\tau\cos\left(\frac{2\pi z}{d}\right)\hat{C}_{20}^1 \quad (31)$$

and

$$\hat{C}^{q}_{L0}(\theta) = \left(\frac{2L+1}{4\pi}\right)^{\frac{1}{2}} \rho_f \sum_{l_1,l} i^l (2l_1+1)^{1/2} (2l+1)^{1/2} P_l(\cos\theta) \times C_g(l_1 L l; 000) \int_0^\infty c_{l_1 L l}(r) j_l(G_q r_{12}) r_{12}^2 dr_{12}. \quad (32)$$

Here, $c_{l_1 L l}(r)$ represents the direct pair correlation function, $C_g(l_1 L l;\ 000)$ are the Clebsch–Gordan coefficients and j_l is the spherical Bessel function of the first kind of order l. Substituting Eq. (22) into Eq. (21) and using the expressions from Eqs. (27)–(30), the grand thermodynamic potential difference between the ordered and isotropic phases can be expressed as

$$-\frac{\Delta W}{N} = -\Delta\rho^* + \frac{1}{2}\Delta\rho^*(2+\Delta\rho^*)\hat{C}^0_{00} + \frac{1}{2}(\tilde{P}_2^2\hat{C}^0_{22} + \tilde{P}_4^2\hat{C}^0_{44}) + \Lambda^2\hat{C}^1_{00} + 2\Lambda\tau\hat{C}^1_{20} + \tau^2\hat{C}^1_{22}, \quad (33)$$

where

$$\hat{C}^{q}_{LL'} = (2L+1)^{1/2}(2L'+1)^{1/2}\rho_f \sum_l i^l \left(\frac{2l+1}{4\pi}\right)^{1/2} \times C_g(LL'l;000) \int_0^\infty c_{LL'l}(r_{12}) j_l(G_q r_{12}) r_{12}^2 dr_{12}. \quad (34)$$

Using the formulation above, phase transitions are determined as follows: at a given temperature, we begin by calculating the body-fixed frame (BF) expansion coefficients of the Mayer function using Eq. (A3), written in the Appendix. These Mayer function expansion coefficients not only enter into the PY equation, but also are used as an initial guess for the direct pair correlation function at low density, starting the iterative cycle for Eqs. (A4) and (A11), again presented in the Appendix. Through this iterative solution, we obtain the values of the BF expansion coefficients $\hat{c}_{l_1 l_2 m}$ for the direct pair correlation function across a range of density values. These expansion coefficients are then converted to their space-fixed frame (SF) counterparts, $\hat{c}_{l_1 l_2 l}$, using Eq. (A9). These values are subsequently used to solve Eqs. (26)–(29) self-consistently to determine the order parameters at a given density. The solution corresponds to the isotropic, nematic, and smectic phases depending on whether all four order parameters are zero, only the orientational order parameters $\tilde{P}_2$ and $\tilde{P}_4$ are non-zero, or all four order parameters are non-zero, respectively. This calculation is repeated for different values of the interlayer spacing d. By substituting these solutions into Eq. (20), we obtain the value of the grand thermodynamic potential difference ΔW between the ordered and isotropic phases, as given by Eq. (33). The phase with the lowest grand potential is considered the stable phase for a given density ρ_f. The transition point is determined by the condition $\Delta W/N = 0$. The nematic-to-smectic A phase transition is determined by comparing the values of $\Delta W/N$ for these two phases at different densities at a given temperature. We recall that, according to the RY-DFT, the calculation is performed at fixed chemical potential and temperature.[79] It may be worth pointing out that in actual calculations, μ_{chem} is not used as an independent control parameter and the input correlations $c_{l_1 l_2 m}(r^*)$ entering the functional are available from liquid-state theory as a function of the isotropic density ρ_f. Therefore, we evaluate the free energies of both the isotropic and ordered phases at the same (μ_{chem}, T), with μ_{chem} implicitly determined by ρ_f through the isotropic equation of state.[76,77] The calculation at each ρ_f is still at fixed (μ_{chem}, T), consistently with the formal RY-DFT criterion. We also compute the inter-layer spacing d for the nematic to smectic A phase transition, identified as the distance at which the grand potential reaches its minimum.

C. Molecular dynamics simulations

MD simulations have been conducted using 1000 GB particles with a dipolar head group strength of $q^* = 1.1$, in a cubic box with periodic boundary conditions. These simulations have employed the Large-scale Atomic/Molecular Massively Parallel Simulator (LAMMPS) open-source software and followed standard protocols, incorporating the long-range dipolar interactions via the Ewald summation method.[86,87] A standard leap-frog algorithm for anisotropic systems has been employed to solve the equations of motion, using a dimensionless MD time step of $\Delta t^* = \sqrt{\frac{m\sigma_0^2}{\epsilon_0}}\Delta t = 0.001$. The reduced temperature $T^* = \frac{k_B T}{\epsilon_0}$ has been regulated using a Nosé–Hoover thermostat with a relaxation time of $\tau_T = 0.1$, where k_B is the Boltzmann constant. We initially have performed NPT simulations on a highly diluted system, adjusting the pressure P to achieve the desired density, η. Next, we have switched to the NVT ensemble and allowed the system to equilibrate for 2×10^6 MD steps at the specified (ρ, T). Finally, we have performed 1×10^4 MD cycles to collect data from the final system configuration, enabling the calculation of the pair correlation function and the second-rank orientational order parameter. The radial distribution function has been computed as

$$g(r) = \frac{1}{4\pi r^2 \rho}\langle \delta(r - r_{12})\rangle_{12}, \quad (35)$$

where r is the radius of a spherical sampling region and $\langle\cdots\rangle_{12}$ denotes a pair average. The second rank orientational order parameter, $\langle P_2\rangle$, has been obtained from the $\mathbf{Q}$ tensor as the maximum eigenvalue of

$$\mathbf{Q}^n_{\alpha\beta} = N^{-1}\sum_i \left(3u_{i\alpha}u_{i\beta} - \frac{\delta_{\alpha\beta}}{2}\right), \quad (36)$$

where $u_{i\alpha}$ is the α Cartesian component of the unit vector defining the orientation of the GB particle i.

IV. RESULTS AND DISCUSSION

We start our investigation by analyzing the local structure of lipid molecules through the calculation of the radial distribution functions $g(r^*)$. In particular, PY predictions are assessed against MD simulations shown in Fig. 3, for a fixed dipole moment head group magnitude of $q^* = 1.1$ and different values of reduced temperature $\left(T^* = \frac{K_b T}{\epsilon_0}\right)$ and density in terms of molecular packing fraction $[\eta = (\pi/6)\rho_f \sigma_0^3 \kappa]$. By looking at the comparison done for $\eta = 0.20$ and $T^* = 1.8$ (A), we first note that the position of the main peak

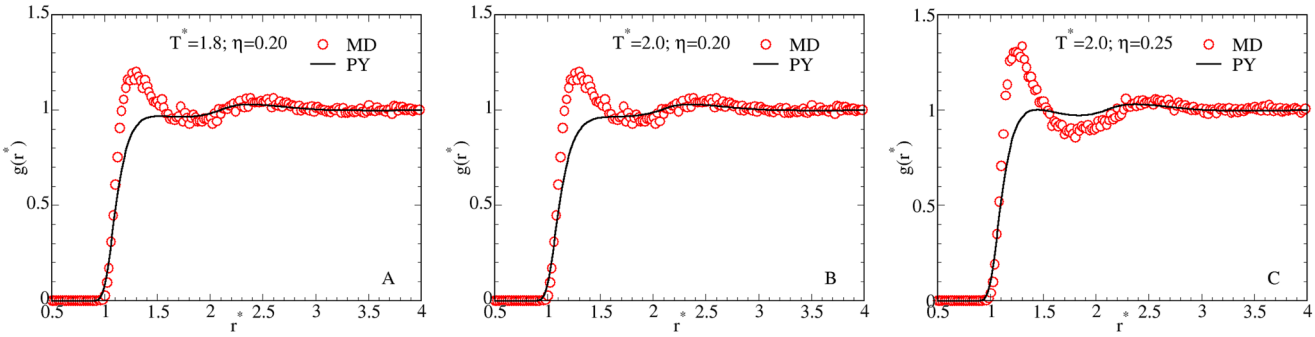

FIG. 3. Comparison between phospholipid $g(r^*)$ obtained by MD simulations (symbols) and PY IET (lines) at constant $q^* = 1.1$. A: T = 1.8, $\eta = 0.20$; B: $T^* = 2.0$, $\eta = 0.20$; and C: $T^* = 2.0$, $\eta = 0.25$.

of $g(r^*)$ predicted by simulations is well caught by the theory, even though its height is underestimated, thus pointing toward a fluid less structured in comparison to MD. Upon increasing the temperature to 2.0, keeping the density unchanged (B), both PY and MD $g(r^*)$ do not show appreciable changes, suggesting that the temperature does not significantly affect the behavior of $g(r^*)$ in the investigated regime. Upon keeping the temperature constant and increasing the density to $\eta = 0.25$ (C), more evident differences between MD and PY emerge: indeed, now the MD $g(r^*)$ shows a well-defined structuring, with a main peak placed at $r^* \approx 1.25$ and a minimum at $r^* \approx 1.80$. Conversely, PY only predicts a small shoulder, followed by a barely noticeable minimum, thus confirming the underestimation of the fluid structuring. On the other hand, the position of the main peak and the first minimum are also well caught in this case.

Once the capability of PY to reproduce essential features (although underestimated) of MD radial distribution functions is clarified, we move to address the impact of the polar-head group strength on the structural properties of phospholipid molecules by analyzing three dipole moment magnitudes ($q^* = 0.5$, 1.1, and 1.5) of GB particles, within PY framework. To this aim, we have evaluated $g(r^*)$ and higher-order harmonics [$g_{220}(r^*)$ and $g_{440}(r^*)$] as a function of both density ($\eta = 0.20, 0.30, 0.40$) and temperature ($T^* = 1.4, 1.6, 1.8$). In Fig. 4, the behavior of $g(r^*)$ shows that the height of its first peak increases with decreasing temperature at fixed densities, indicating enhanced local molecular ordering due to stronger dipolar interactions at lower temperatures. This effect becomes more pronounced at higher densities, reflecting tighter molecular packing and stronger intermolecular interactions. Interestingly, at lower densities ($\eta = 0.20$), the peak heights are almost identical for all three dipole strengths, suggesting that the influence of dipole moment on molecular ordering is relatively minor at reduced densities.

In Fig. 5, the pair correlation functions of phospholipid molecules are plotted for four reduced temperatures ranging from 1.4 to 2.0 while varying the dipolar head group strength ($q^* = 0.5$,

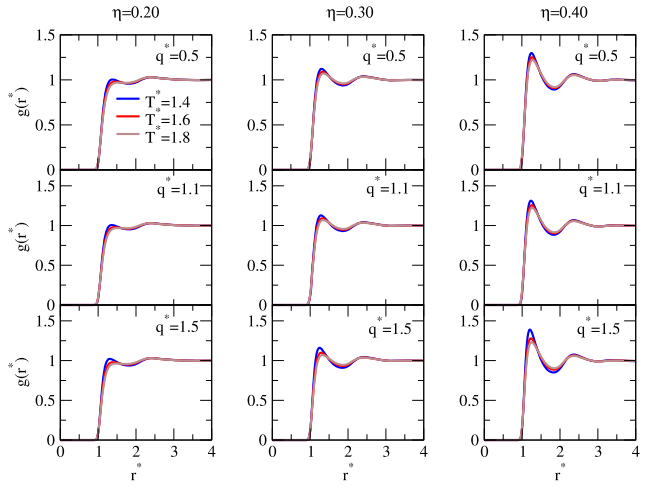

FIG. 4. PY pair correlation functions of phospholipid molecules with different head group dipole moments for three temperatures ($T^* = 1.4$, 1.6, and 1.8) and densities ($\eta = 0.20$, 0.30, and 0.40).

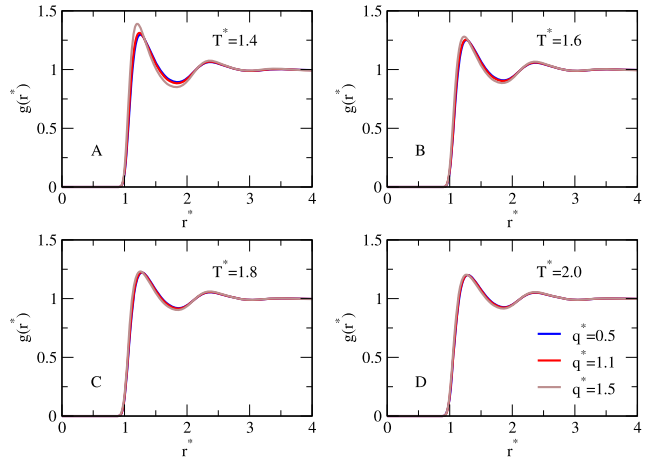

FIG. 5. PY pair correlation functions of phospholipid molecules with different head group dipole moments for three different temperatures ($T^* = 1.4$, 1.6, and 1.8) at fixed $\eta = 0.40$.

1.0, 1.5) at a fixed density ($\eta = 0.40$). At lower temperatures ($T^* = 1.4$ and 1.6), the peak height of the pair correlation function is higher for phospholipids with stronger dipolar interactions ($q^* = 1.5$) compared to those with weaker dipole moments ($q^* = 0.5$ and 1.0). This suggests that a stronger dipole moment enhances the effective attractive interactions between the ellipsoids, leading to a more pronounced local ordering. However, at higher temperatures ($T^* = 1.8$ and 2.0), the peak heights of $g(r^*)$ converge and become nearly identical for all dipole strengths, indicating that thermal fluctuations dominate at elevated temperatures, reducing the influence of dipolar interactions on molecular organization.

Figure 6 delves deeper into molecular alignment by presenting higher-order harmonics, $g_{220}(r^*)$ (A) and $g_{440}(r^*)$ (B), defined in the Appendix, for the system at $\eta = 0.40$ and $T^* = 1.5$ for different head group dipole moments. These higher-order harmonics exhibit trends similar to the radial distribution functions, underscoring consistent structural behavior across correlation measures. We observe that the peak height of $g_{220}(r^*)$ for the weaker dipole strength ($q^* = 0.5$) is significantly lower than for the stronger dipoles ($q^* = 1.1$ and 1.5), suggesting that systems with lower dipole moments require a higher density or a lower temperature to achieve the ordered (nematic) phase. These results highlight that the dipole strength enhances molecular ordering and that higher-order harmonics provide valuable insights into the onset of orientationally ordered phases. These findings underscore the intricate relationship between dipole strength, density, and temperature in determining the structural organization of phospholipid systems.

In order to complete our analysis of the structure of the phospholipid molecules, we turn our attention to analyze the static structure factor $s(k^*)$ of the system (see the Appendix for its definition). In Fig. 7, we plot the static structure factor for three different values of dipole moments ($q^* = 0.5, 1.1, 1.5$), densities ($\eta = 0.20, 0.30, 0.40$), and temperatures ($T^* = 1.4, 1.6, 1.8$). In all cases, $s(k^*)$ show a regular structure with a principal peak that changes only slightly with temperature. It is worth noting that in none of these plots, $s(k^*)$ diverges in the limit $k \to 0$. This leads us to conclude that the system is thermodynamically stable for these combinations of parameters in PY theory and that there are no tendencies for spontaneous liquid–vapor phase separation. In addition, it may be worth noting that for $\eta^* = 0.40$, a small shoulder arises for low wavevectors ($k^* \simeq 5$), compatibly with the first appearance of inhomogeneities [also known as intermediate range order (IRO)] in the system.[88,89] In agreement with indications provided by higher-order harmonics, it emerges that this shoulder appears slightly more defined upon increasing q^*, thus confirming that a high dipole strength enhances molecular ordering.

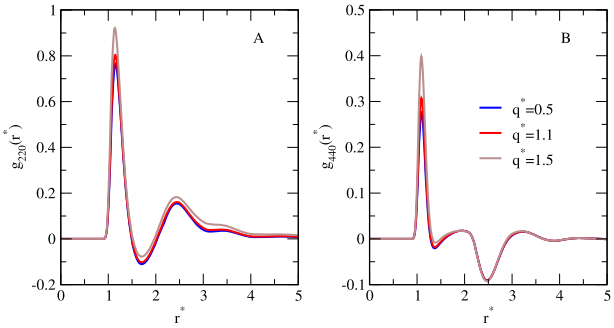

FIG. 6. Higher-order harmonics $g_{220}(r^*)$ (A) and $g_{440}(r^*)$ (B) obtained from the expansion of PY radial distribution functions for three different dipole moments.

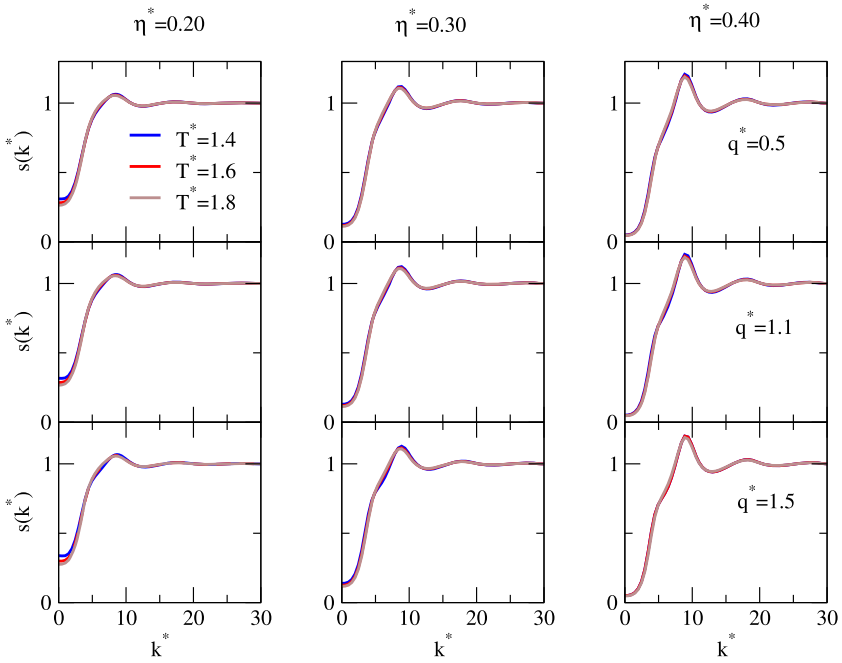

FIG. 7. Behavior of PY static structure factors of phospholipid molecules with different head group dipole moments for three temperatures ($T^* = 1.4, 1.6, 1.8$) and densities ($\eta = 0.20, 0.30, 0.40$).

TABLE I. Freezing transition parameters calculated for three different dipolar head groups.

T^*	q^*	Transition	η	d^*	$\Delta\eta$	$\tilde{P}_2$	$\tilde{P}_4$	Λ	τ	Π
1.40	0.5	I-N	0.348	0	0.26	0.82	0.57	0	0	1.35
		N-Sm-A	0.394	3.25	0.28	0.99	0.87	0.52	0.51	2.05
	1.1	I-N	0.334	0	0.23	0.83	0.59	0	0	1.26
		N-Sm-A	0.375	3.35	0.32	0.99	0.95	0.53	0.51	1.86
1.60	0.5	I-N	0.403	0	0.10	0.77	0.51	0	0	2.40
		N-Sm-A	0.456	2.95	0.12	0.93	0.76	0.51	0.52	3.92
	1.1	I-N	0.389	0	0.14	0.78	0.52	0	0	2.02
		N-Sm-A	0.444	3.09	0.14	0.95	0.77	0.47	0.48	3.34
	1.5	I-N	0.356	0	0.23	0.81	0.56	0	0	1.48
		N-Sm-A	0.401	3.17	0.23	0.99	0.86	0.67	0.67	2.23
1.80	0.5	I-N	0.452	0	0.06	0.75	0.47	0	0	3.88
	1.1	I-N	0.439	0	0.07	0.76	0.48	0	0	3.41
		N-Sm-A	0.492	2.86	0.09	0.89	0.74	0.59	0.60	5.55
	1.5	I-N	0.410	0	0.10	0.77	0.50	0	0	2.57
		N-Sm-A	0.485	3.03	0.09	0.88	0.73	0.46	0.49	4.98
2.00	0.5	I-N	0.496	0	0.04	0.74	0.46	0	0	5.94
	1.1	I-N	0.486	0	0.04	0.74	0.46	0	0	5.35
	1.5	I-N	0.456	0	0.06	0.75	0.47	0	0	4.06
		N-Sm-A	0.532	2.78	0.04	0.84	0.67	0.40	0.43	7.79
2.20	0.5	I-N	0.534	0	0.03	0.73	0.45	0	0	8.75
	1.1	I-N	0.534	0	0.03	0.73	0.45	0	0	7.87
	1.5	I-N	0.502	0	0.04	0.73	0.45	0	0	6.10

Once structural analysis is completed, we now make use of the DFT formalism, as outlined before, to investigate liquid crystalline phase transitions in the system. In particular, we focus on identifying the isotropic–nematic and nematic–smectic A freezing transitions. Our aim is to calculate the freezing parameters across a range of reduced temperatures, $1.4 \leq T^* \leq 2.2$. Since the DFT methodology requires as input the pair correlation functions of a reference isotropic fluid, it follows that the accuracy of the calculated transition parameters depends heavily on the approximation used to estimate these pair correlations.[65] The results, detailing the DFT freezing parameters [calculated according to Eqs. (26)–(29)] are systematically presented in Table I. These findings provide insights into the way how variations in head group strength and reduced temperature influence the onset of liquid crystalline phase transitions, a critical issue for understanding the ordering behavior of phospholipid molecules in different thermodynamic regimes.

As a general trend, we observe that the orientational order parameters ($\tilde{P}_2$ and $\tilde{P}_4$) are significantly higher during the nematic–smectic A (N–Sm-A) transition than in the isotropic–nematic (I–N) transition, according to the more ordered structure expected in the smectic A phase. In addition, the mixed (τ) and translational (Λ) order parameters are nonzero only for the N–Sm-A transition, highlighting the emergence of layered arrangements and translational order in the smectic A phase. We also compute the compressibility pressure Π, which quantifies how much a given material changes its volume in response to an applied force. Since this parameter provides information on membrane stiffness, elasticity, and phase behavior, it is essential in many biophysical investigations. More details on the way to compute Π can be found in the Appendix. From Table I, we note that Π increases with temperature and becomes higher for Sm-A transitions, indicating an increase of the rigidity in the smectic phase.

For the lowest temperature investigated (i.e., $T^* = 1.4$), we observe that for $q^* = 0.5$, the density for which the I–N phase transition takes place is $\eta = 0.348$, while the N-Sm-A transition is expected for $\eta = 0.394$. Upon increasing q^* to 1.1, the transition density slightly decrease, suggesting that the higher dipole moment promotes structuring. On the other hand, no stable nematic or smectic A phase for the dipole moment $q^* = 1.5$ is found. This apparent contradiction can be explained by taking into account that the dipolar strength enhances structuring mainly at the local scale, with possible destabilization of global mesophases when the low-temperature region is approached. Finally, we anticipate that densities at which phase transitions occur are typically lower than those found for higher temperatures. Indeed, in the latter case, the entropic contribution plays a significant role, hampering the molecular ordering, which, therefore, can be obtained only by increasing the density.

For intermediate temperatures ($T^* = 1.6$ and $T^* = 1.8$), the I–N transition densities show modest increases compared to $T^* = 1.4$, while the orientational order parameters keep values comparable with those already found for the lowest temperature. On the other hand, in this temperature regime, both I–N and N–Sm-A transitions are found for $q^* = 1.5$. In particular, for $T^* = 1.6$, the

orientational order parameter ($\tilde{P}_2$) for $q^* = 1.5$ during the N–Sm-A transition reaches 0.99, suggesting strong alignment of particles. We also observe that the change in density ($\Delta\eta$) between the isotropic and nematic phases decreases upon increasing the temperature. The trends are consistent for all head group strengths, but higher q^* values exhibit higher order (higher $\tilde{P}_2$, $\tilde{P}_4$) during the transitions, according to the stronger dipolar interactions.

For high temperatures ($T^* = 2.0$ and $T^* = 2.2$), the transitions occur at significantly high densities and the differences in density between phases is reduced, especially for the I–N transition. The order parameters $\tilde{P}_2$ and $\tilde{P}_4$ show low values, suggesting a weaker molecular alignment due to the increased thermal motion. For the N–Sm-A transition, the translational (Λ) and mixed (τ) order parameters are smaller than those found for lower temperatures, indicating a reduced structural order in the smectic phase. We finally observe that for the highest temperature investigated (i.e., $T^* = 2.2$), no N–Sm-A transition is found, thus signaling that the entropic contribution is too high to allow the development of such an ordered phase.

In Table II, we compare DFT and MD parameters for the N–Sm-A phase transition for three different temperatures, ranging from $T^* = 1.4$ to $T^* = 1.8$, with a fixed polar head group strength $q^* = 1.1$. We observe that at fixed temperature, theoretical estimates of orientational order parameters $\tilde{P}_2$ reasonably agree with MD data. However, theoretical predictions of translational order parameters μ typically underestimate the corresponding MD results, but for the highest temperature considered (namely, $T^* = 2.0$). This discrepancy arises because translational transition parameters in the theory are derived from classical DFT, where the harmonics of the correlation function, coming from the liquid-state IET, are used as input. Typical microscopic configurations obtained from MD simulations for fluid phases and fluid layered phases with $q^* = 1.1$ under different thermodynamic state points are given in Fig. 8. In particular, we have verified that in panel A, the orientational order parameter is ~0.03 and such a low value is indicative of an isotropic phase. Conversely, in panel B, the orientational order parameter attains a value of 0.58, while the translational order parameter is zero, thus pointing toward a nematic phase. Finally, in panel C, the contemporary existence of both the orientational and translational order parameters, with respective values of 0.99 and 0.95, indicates the Sm-A phase.

Using Table I, it is possible to draw DFT phase diagrams in the temperature-density plane. In particular, we report in Fig. 9, the portion of the phase diagram showing I and N phase regions, while varying the dipolar head group strength. From this diagram, it emerges that the I–N transition occurs at progressively lower densities as the dipolar head group strength increases. This decrease in the transition density is less pronounced when going from $q^* = 0.5$

TABLE II. Comparison between DFT and MD parameters for the N–Sm-A phase transition.

	T^*	q^*	η	$\tilde{P}_2$	Λ
DFT	1.40	1.1	0.375	0.99	0.51
MD			0.369	0.99	0.70
DFT	1.60	1.1	0.444	0.95	0.48
MD			0.447	0.98	0.80
DFT	1.80	1.1	0.492	0.89	0.60
MD			0.492	0.98	0.50
DFT	2.00	1.1	0.486	0.76	⋯
MD			0.476	0.96	0.85

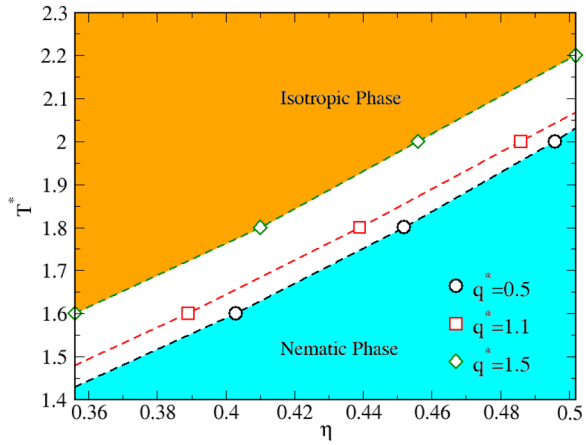

FIG. 9. DFT results for the I–N phase transition of phospholipids in the T^*–η plane for the different dipolar strengths investigated.

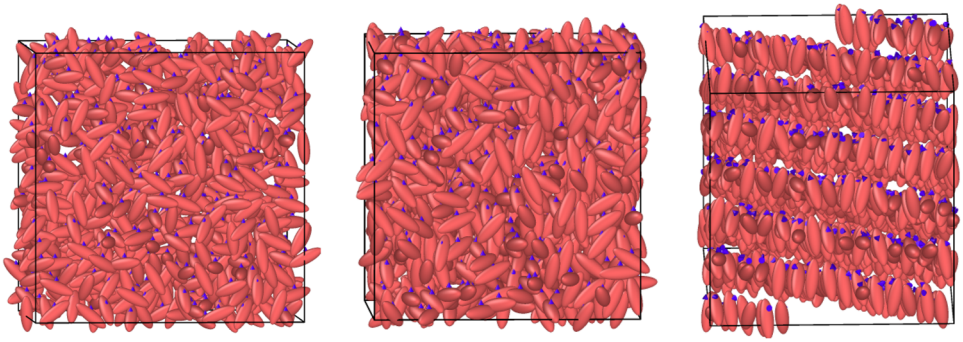

A: $T^* = 1.80, \eta = 0.20$ B: $T^* = 2.20, \eta = 0.32$ C: $T^* = 1.40, \eta = 0.56$

FIG. 8. Snapshots of configurations generated by MD simulations for $q^* = 1.1$ and different thermodynamic conditions, corresponding to different mesophases. A: isotropic; B: nematic; and C: smectic A.

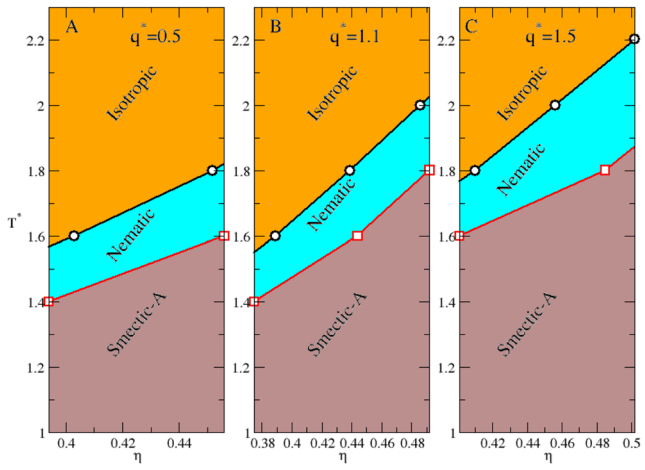

FIG. 10. DFT phase diagram of phospholipids in the T^*–η plane for $\mu^* = 0.5$ (A), 1.1 (B), and 1.5 (C).

to $q^* = 1.1$ rather than from $q^* = 1.1$ to $q^* = 1.5$, suggesting a nonlinear dependence of the transition density on the dipolar strength. As a consequence, for a fixed density, upon increasing dipolar head group strength, the I–N transition shifts to lower temperatures. In addition, the phase diagram reveals that the nematic phase emerges at progressively lower densities as q^* increases from 0.5 to 1.5, emphasizing the role of dipolar interactions in stabilizing ordered phases even under such conditions.

In order to better highlight the role played by the dipole moment in determining the final behavior of the lipid system, we show in Fig. 10 three different phase diagrams, each one corresponding to a given value of q^*, including also the Sm–A phase. It clearly emerges that upon increasing q^*, the temperature range of stability of both nematic and Sm-A phase increases as well. At the same time, the transitions from the isotropic phase to the nematic phase and from the nematic phase to the smectic A phase shift to higher temperatures. Furthermore, it may be worth pointing out that this scenario only partially agrees with MD simulations: indeed, due to the PY underestimation of the fluid structuring discussed apropos radial distribution functions, the theory predicts an isotropic phase for densities where, according to MD, we should expect a nematic phase.

V. CONCLUSIONS

In this study, we have systematically investigated the structure and phase behavior of phospholipid molecules using Percus–Yevick (PY) integral equation theory (IET) and density functional theory (DFT) under different conditions of temperature, density, and dipolar strength. For some values of these parameters, theoretical predictions have been assessed against molecular dynamics (MD) simulations performed through LAMMPS software. The comparison of pair correlation functions $g(r^*)$ between PY-IET and MD simulations shows qualitative agreement for low density ($\eta = 0.20$) at fixed temperatures ($T^* = 1.8$ and 2.0). The agreement worsens upon increasing η, with MD predicting a progressive structuring of the fluid not caught by PY. In addition, cooling down the system from $T^* = 2.0$ to 1.8 has a little effect on its structure.

The role played by dipolar head group strength ($q^* = 0.5$, 1.1, 1.5) on the structural organization has been further examined through higher-order harmonics [$g_{220}(r^*)$, $g_{440}(r^*)$] across different densities ($\eta = 0.20, 0.30, 0.40$) and temperatures ($T^* = 1.4$, 1.6, 1.8, 2.0). The results demonstrate that strong dipolar interactions enhance molecular ordering, particularly at low temperatures and high densities, as evidenced by pronounced peak heights. For high temperatures ($T^* \geq 1.8$), the influence of dipole strength diminishes due to thermal fluctuations. In addition, the static structure factor analysis reveals a consistent principal peak across different temperatures, dipole moments, and densities, indicating minimal temperature dependence. In addition, the absence of divergence in $S(k^*)$ as $k \to 0$ confirms the thermodynamic stability of the system without tendencies for a liquid–vapor phase separation under the studied conditions. On the other hand, the existence of a shoulder at high density (progressively more defined upon increasing q^*) points toward the onset of an intermediate range order in the system.

Once the fluid structure of the system is investigated, we employed DFT analysis, taking structural inputs from PY, in order to obtain estimations about isotropic–nematic (I–N) and nematic–smectic A (N–Sm-A) transition parameters. It emerges that both temperature and dipolar head group strength play a significant role in promoting ordering: indeed, transition at low T^* and high q^* may occur at low densities, since under these conditions ordering is favored and also aligned and layered structures can be easily formed. Compressibility pressure and order parameters further underscore the emergence of greater rigidity and structural organization in the ordered phases and, in particular, in the smectic A phase. For high temperatures ($T^* = 2.0$ and 2.2), transitions occur at high densities, with low values of order parameters and minimal density differences, highlighting the dominance of thermal fluctuations. Collectively, these findings may help understand how dipolar interactions, density, and temperature drive the structural organization and phase transitions of phospholipid systems, offering valuable insights into their thermodynamic behavior across different regimes. Similar trends also emerge from the comparison between DFT and MD transition parameters for $q^* = 1.1$ and temperatures ranging from $T^* = 1.4$ to $T^* = 1.8$. On the other hand, translational order parameters are typically underestimated by the theory.

Future improvements rely on a systematic PY-IET study taking into account different dipole orientations, which would be representative of a more realistic phospholipid model. In addition, the implementation of more refined input for the DFT would better take into account the progressive structuring of the system upon increasing the density. We also plan to explicitly include the solvent to investigate solvent–lipid interactions, such as hydration properties. Further applications of our formalism, including the possibility to investigate the self-assembly of phospholipids in other kinds of mesophases, are currently under scrutiny.

ACKNOWLEDGMENTS

We acknowledge financial support from the National Recovery and Resilience Plan (NRRP), Mission 4, Component 2, Investment 1.1, Call for Tender No. 104 PRIN 2022 published on 2 February

2022 by the Italian Ministry of University and Research (MUR), funded by the European Union—NextGenerationEU—Project Title "Unveiling the mutual interaction between lipid rafts and amyloid oligomers at the neuronal membrane—NeuRaftAmyl," Grant No. CUP J53D23001320006. We acknowledge the CINECA award under the ISCRA initiative, for the availability of high performance computing resources and support. The authors thank Tanay Paul for helpful scientific discussions.

AUTHOR DECLARATIONS

Conflict of Interest

The authors have no conflicts to disclose.

Author Contributions

Sahire Azam Ansary: Formal analysis (lead); Investigation (lead); Methodology (lead); Writing – original draft (lead). **Gianmarco Munaò**: Conceptualization (equal); Data curation (equal); Supervision (equal); Writing – review & editing (equal). **Valeria Conti Nibali**: Conceptualization (equal); Data curation (equal); Funding acquisition (lead); Supervision (equal); Writing – review & editing (equal).

DATA AVAILABILITY

The data that support the findings of this study are available from the corresponding authors upon reasonable request.

APPENDIX: EXPANSION OF ORNSTEIN–ZERNIKE INTEGRAL EQUATION THEORY INTO SPHERICAL HARMONICS

In this appendix, we report details concerning the way how PY can be expanded into spherical harmonics in order to be implemented inside the GB framework. Since the correlation functions in an isotropic fluid are rotationally invariant and depend only on pairwise interactions, they can be expanded using a rotationally invariant basis set. In the SF coordinate frame, this expansion can be expressed as

$$\psi^{(2)}(\mathbf{r}_{12},\boldsymbol{\Omega}_1,\boldsymbol{\Omega}_2)=\sum_{l_1l_2l}\psi_{l_1l_2l}(r)\sum_{m_1m_2m}C_g(l_1l_2l;m_1m_2m)\times Y_{l_1m_1}(\boldsymbol{\Omega}_1)Y_{l_2m_2}(\boldsymbol{\Omega}_2)Y^*_{lm}(\hat{\mathbf{r}}). \quad \text{(A1)}$$

Here, $\psi^{(2)}$ represents any pair function, $C_g(l_1l_2l;\ m_1m_2m)$ are the Clebsch–Gordan coefficients, Y_{lm} denote the spherical harmonics, and $\psi_{l_1l_2l}$ are the reduced expansion coefficients. In the BF frame, where the intermolecular vector $\mathbf{r}_{12}$ aligns with the z axis of the SF frame, the expansion can be expressed as

$$\psi^{(2)}(\mathbf{r}_{12},\boldsymbol{\Omega}_1,\boldsymbol{\Omega}_2)=\sum_{l_1l_2m}\psi_{l_1l_2m}(r)Y_{l_1m}(\boldsymbol{\Omega}_1)Y_{l_2\underline{m}}(\boldsymbol{\Omega}_2), \quad \text{(A2)}$$

with $\underline{m}=-m$. The expansion coefficients $\psi_{l_1l_2m}(r)$ are defined as

$$\psi_{l_1l_2m}(r_{12})=\int d\boldsymbol{\Omega}_1 d\boldsymbol{\Omega}_2\psi^{(2)}(\mathbf{r},\boldsymbol{\Omega}_1,\boldsymbol{\Omega}_2)Y^*_{l_1m}(\boldsymbol{\Omega}_1)Y^*_{l_2\underline{m}}(\boldsymbol{\Omega}_2). \quad \text{(A3)}$$

Taking the Fourier transform of the angle-dependent function $h^{(2)}(\mathbf{r}_{12},\ \Omega_1,\ \Omega_2)$ $(c^{(2)}(\mathbf{r}_{12},\ \Omega_1,\ \Omega_2))$ appearing in the OZ equation, we obtain

$$\psi^{(2)}(\mathbf{r}_{12},\boldsymbol{\Omega}_1,\boldsymbol{\Omega}_2)=\left(\frac{1}{2\pi}\right)^3\int d\mathbf{k}\,\exp(i\mathbf{k}.\mathbf{r}_{12})\psi^{(2)}(\mathbf{k},\boldsymbol{\Omega}_1,\boldsymbol{\Omega}_2), \quad \text{(A4)}$$

where $\psi^{(2)}(\mathbf{k},\boldsymbol{\Omega}_1,\boldsymbol{\Omega}_2)=\int d\mathbf{r}_{12}\exp(ik\cdot\mathbf{r}_{12})\psi^{(2)}(\mathbf{r}_{12},\boldsymbol{\Omega}_1,\boldsymbol{\Omega}_2)$ and, when substituted into the OZ equation, the integral over r, which represents a convolution in real space, becomes a product in the Fourier space which takes the following expression:

$$h^{(2)}(\mathbf{k},\boldsymbol{\Omega}_1,\boldsymbol{\Omega}_2)=c^{(2)}(\mathbf{k},\boldsymbol{\Omega}_1,\boldsymbol{\Omega}_2)+\rho_f\int d\boldsymbol{\Omega}_3 c^{(2)}(\mathbf{k},\boldsymbol{\Omega}_1,\boldsymbol{\Omega}_3)h^{(2)}(\mathbf{k},\boldsymbol{\Omega}_3,\boldsymbol{\Omega}_2). \quad \text{(A5)}$$

Due to this simplification of the OZ equation, working in the Fourier space becomes computationally advantageous. By substituting the BF spherical harmonic expansion for all angle-dependent functions, the OZ equation reduces to a set of algebraic equations in the Fourier space,

$$\hat{h}_{l_1l_2m}(k)=\hat{c}_{l_1l_2m}(k)+(-1)^m\frac{\rho_f}{4\pi}\sum_{l_3}\hat{c}_{l_1l_3m}(k)\hat{h}_{l_3l_2m}(k). \quad \text{(A6)}$$

This form of OZ equation is simple in structure and easy to use in practice. The harmonic coefficients in the real and Fourier space are related through mutual Hankel transforms,[90]

$$\hat{\psi}_{l_1l_2m}(k)=4\pi i^l\int_0^\infty dr r^2 j_k(kr)\hat{\psi}_{l_1l_2m}(r_{12}), \quad \text{(A7)}$$

$$\hat{\psi}_{l_1l_2l}(r_{12})=\frac{4\pi}{(2\pi)^3}i^l\int_0^\infty dk k^2 j_k(kr)\hat{\psi}_{l_1l_2l}(k), \quad \text{(A8)}$$

where $j_l(kr_{12})$ is the spherical Bessel function. The harmonics in the Fourier space are related to those in the space-fixed frame by

$$\hat{\psi}_{l_1l_2l}(k)=\sum_m\sqrt{\frac{4\pi}{2l+1}}Cg(l_1l_2l;m\underline{m}0)\hat{\psi}_{l_1l_2m}(k) \quad \text{(A9)}$$

and

$$\hat{\psi}_{l_1l_2m}(k)=\sum_l\sqrt{\frac{2l+1}{4\pi}}Cg(l_1l_2l;m\underline{m}0)\hat{\psi}_{l_1l_2l}(k). \quad \text{(A10)}$$

The angular functions in the PY closure in Eq. (13) can also be expanded in the BF frame, obtaining,

$$c_{l_1l_2m}(r_{12})=\sum_{l_1'l_1''l_2'l_2''}\frac{1}{4\pi}\sqrt{\frac{(2l_1'+1)(2l_2'+1)(2l_1''+1)(2l_2''+1)}{(2l_1+1)(2l_2+1)}}\times Cg(l_1'l_1''l_1;000)Cg(l_2'l_2''l_2;000)\times\sum_{m'm''}Cg(l_1'l_1''l_1;m'm''m)Cg(l_2'l_2''l_2;\underline{m}'\underline{m}''\underline{m})\times f_{l_1'l_2'm'}(r_{12})[4\pi\delta_{000}^{l_2'l_2''m''}+\gamma_{l_2'l_2''m''}(r_{12})], \quad \text{(A11)}$$

where $\gamma_{l_2'l_2''m''}(r_{12})=h_{l_2'l_2''m''}(r_{12})-c_{l_2'l_2''m''}(r_{12})$; the summation is over allowed values of the indices.

TABLE III. Terms included in the basis sets in SF and BF harmonics expansion.

Basis set		Terms included								
SF (l_{max} = 8)	33	000	202	220	242	404	440	222	240	442
		224	426	444	446	606	264	266	462	464
		466	660	662	664	666	286	484	486	682
		684	686	880	882	884	886			
BF (l_{max} = 8)	54	000	020	220	240	040	440	060	260	460
		660	280	480	680	880	221	241	441	261
		461	661	281	481	681	881	222	242	442
		262	462	662	282	482	682	882	443	463
		663	483	683	883	444	464	664	484	684
		884	665	685	885	666	686	886	887	888

In principle, the indices l_i vary from 0 to ∞ and $-l_i \le m_i \le l_i$, amounting to an infinite number of expansion coefficients. However, in practical calculations, the series is usually truncated at $l_i \le l_{max}$, whose value depends on the anisotropy of the pair functions and the density of the system. Pair correlation functions are obtained by solving the OZ equation (20) and the PY equation (25) self consistently. It is important to note that in any numerical solution of the OZ equation, the accuracy of the results relies on the number of spherical harmonic coefficients used for each orientation-dependent function. As the anisotropy in molecular shape (or in interactions) and the fluid density ρ_f increase, higher-order harmonic coefficients are required to achieve proper convergence. In the present case of phospholipid molecules, due to the anisotropy in molecular shape, we truncate the spherical harmonic expansion of angle-dependent functions at l_{max} = 8. The following conditions apply on the expansion coefficients: (i) due to the presence of Clebsch–Gordan coefficients in Eq. (15), only coefficients that satisfy the conditions $m = m_1 + m_2$ and $|l_1 - l_2| \le l \le l_1 + l_2$ contribute to the sum; (ii) due to the rotational invariance of the isotropic fluid, only coefficients with even number of $l_1 + l_2 + l$ enter the expansion; and (iii) the axially symmetric nature of the GB molecule puts the constraints that every single l has to be even. Under these conditions, the series expansion includes a total of 54 BF (or 33 SF) harmonic coefficients, as detailed in Table III. We found that, with these number of harmonics, the self-consistent iterative solution of OZ and PY converges up to the accuracy of 10^{-5} in the range of density of our interest. Using PY, we have calculated the radial distribution function $g(r^*) = 1 + h_{000}(r^*)/4\pi$ and the higher order harmonics $g_{220}(r^*) = \frac{h_{220}(r^*)}{4\pi}$ and $g_{440}(r^*) = \frac{h_{440}(r^*)}{4\pi}$ at different temperatures T^* and densities η. The Fourier transform of the pair correlation function gives the structure factor $S(k^*) = 1 + \rho_f \int \exp(-i\mathbf{k}\cdot\mathbf{r}) g(r^*)$. The numerical procedure for solving Eqs. (20) and (25) follows the same approach outlined in Ref. 91.

The isothermal compressibility of the fluid is defined by

$$\frac{\partial}{\partial \rho_f}\left(\beta P^c\right) = 1 - \rho_f \int d\mathbf{\Omega}_1\, d\mathbf{\Omega}_2\, dr_{12}\, c(\mathbf{r}_{12}, \mathbf{\Omega}_1, \mathbf{\Omega}_2). \tag{A12}$$

On expanding Eq. (A12) in spherical harmonics in the SF frame and after simplification, we get

$$\frac{\partial}{\partial \rho}\left(\beta P^c\right) = 1 - \hat{C}^0_{00}, \tag{A13}$$

where

$$\hat{C}^0_{00} = \frac{\rho}{4\pi} \int r^2\, c_{000}(r_{12})\, dr_{12}. \tag{A14}$$

The compressibility pressure is then obtained by integrating Eq. (A13),

$$\frac{\beta P^c}{\rho} = 1 - \frac{1}{\rho}\int_0^\rho \hat{C}^0_{00}[\rho']\, d\rho'. \tag{A15}$$

The reduced compressibility pressure can be written as

$$\Pi = \frac{P^c \sigma_0^3}{\epsilon_0}. \tag{A16}$$

REFERENCES

[1] C. V. Kulkarni, Nanoscale **4**, 5779 (2012).
[2] G. van Meer, D. R. Voelker, and G. W. Feigenson, Nat. Rev. Mol. Cell Biol. **9**, 112 (2008).
[3] Y. N. Kaznessis, S. Kim, and R. G. Larson, Biophys. J. **82**, 1731 (2002).
[4] A. Ali, T. Dou, A. P. Holman, A. Hung, L. Osborne, D. Pickett, A. Rodriguez, K. Zhaliazka, and D. Kurouski, Biophys. Chem. **306**, 107174 (2024).
[5] P. R. Cullis and B. de Kruijff, Biochim. Biophys. Acta **559**, 399 (1979).
[6] J. N. Israelachvili, *Intermolecular and Surface Forces* (Academic Press, 2011).
[7] K. Gawrisch *et al.*, Biophys. J. **61**, 1213 (1992).
[8] P. Jurkiewicz, L. Cwiklik, A. Vojtíšková, P. Jungwirth, and M. Hof, Biochim. Biophys. Acta **1818**, 609 (2012).
[9] H. S. Antila, A. Wurl, O. H. S. Ollila, M. S. Miettinen, and T. M. Ferreira, Biophys. J. **121**, 68 (2022).
[10] T. Paul and J. Saha, Phys. Rev. E **95**, 062703 (2017).
[11] A. A. Gurtovenko, J. Chem. Phys. **122**, 244902 (2005).
[12] P. T. Vernier, M. J. Ziegler, and R. Dimova, Langmuir **25**, 1020 (2009).
[13] H. Brockman, Chem. Phys. Lipids **73**, 57 (1994).
[14] S. Sullivan and H. Herma, Neurology **42**, 1992 (1992).
[15] L. N. Handly, J. Yao, and R. Wollman, J. Mol. Biol. **428**, 3669 (2016).
[16] R. Mezzenga, J. M. Seddon, C. J. Drummond, B. J. Boyd, G. E. Schröder-Turk, and L. Sagalowicz, Adv. Mater. **31**, 1900818 (2019).
[17] V. P. Chavda, S. Dyawanapelly, S. Dawre, I. Ferreira-Faria, R. Bezbaruah, N. R. Gogoi, P. Kolimi, D. J. Dave, A. C. Paiva-Santos, and L. K. Vora, Int. J. Pharm. **647**, 123546 (2023).
[18] C. Guo, J. Wang, F. Cao, R. J. Lee, and G. Zhai, Drug Discovery Today **15**, 1032 (2010).
[19] D. H. Kim, A. Jahn, S. J. Cho, J. S. Kim, M. H. Ki, and D. D. Kim, J. Pharm. Invest. **45**, 1 (2015).
[20] S. Chandrasekhar, *Liquid Crystals*, 2nd ed. (Cambridge University Press, Cambridge, 1977).
[21] P. G. de Gennes and J. Prost, *The Physics of Liquid Crystals*, 2nd ed. (Oxford University Press, New York, 1993).
[22] Y. Huang and S. Gui, RSC Adv. **8**, 6978 (2018).
[23] J. D. Du, W. K. Fong, S. Salentinig, S. M. Caliph, A. Hawley, and B. J. Boyd, Phys. Chem. Chem. Phys. **17**, 14021 (2015).
[24] L. A. Bulavin, D. V. Soloviov, V. I. Gordeliy, O. S. Svechnikova, A. O. Krasnikova, N. A. Kasian, O. V. Vashchenko, and L. N. Lisetski, Phase Transitions **88**, 582 (2015).
[25] A. M. Dattelbaum, G. A. Montano, A. Roco, A. P. Shreve, and S. Iyer, NSTI-Nanotech. **2**, 480 (2008).
[26] H. Fernández-Morán, Rev. Mod. Phys. **31**, 319 (1959).

[27]K. Liu, D. Chen, A. Marcozzi, L. Zheng, J. Su, D. Pesce, W. Zajaczkowski, A. Kolbe, W. Pisula, K. Müllen, N. A. Clark, and A. Herrmann, Proc. Natl. Acad. Sci. U. S. A. **111**, 18596 (2014).
[28]R. Hashim, N. I. Zahid, N. F. Aripin, S. Ogawa, and A. Sugimura, J. Oleo Sci. **67**, 651 (2018).
[29]J. W. Goodby, V. Görtz, S. J. Cowling, G. Mackenzie, P. Martin, D. Plusquellec, T. Benvegnu, P. Boullanger, D. Lafont, Y. Queneau, and S. Chambert, Chem. Soc. Rev. **36**, 1971 (2007).
[30]Å. A. Skjevik, B. D. Madej, C. J. Dickson, K. Teigen, R. C. Walker, and I. R. Gould, Chem. Commun. **51**, 4402 (2015).
[31]L. Gai, K. A. Maerzke, P. T. Cummings, and C. McCabe, J. Chem. Phys. **137**, 144901 (2012).
[32]M. Ramezanpour, M. L. Schmidt, B. Y. M. Bashe, J. R. Pruim, M. L. Link, P. R. Cullis, P. E. Harper, J. L. Thewalt, and D. P. Tieleman, Langmuir **36**, 6668 (2020).
[33]S. J. Marrink, A. H. De Vries, and A. E. Mark, J. Phys. Chem. B **108**, 750 (2004).
[34]S. J. Marrink and A. E. Mark, Biophys. J. **87**, 3894 (2004).
[35]D. Demurtas, P. Guichard, I. Martiel, R. Mezzenga, C. Hébert, and L. Sagalowicz, Nat. Commun. **6**, 8915 (2015).
[36]L. Powers and N. A. Clark, Proc. Natl. Acad. Sci. U. S. A. **72**, 840 (1975).
[37]P. Garidel, Y. Kaconis, L. Heinbockel, M. Wulf, S. Gerber, A. Munk, V. Vill, and K. Brandenburg, Open Biochem. J. **9**, 49 (2015).
[38]Z. Xu, W. Wang, Y. Cao, and B. Xue, Supramol. Mater. **2**, 100049 (2023).
[39]B. Wang, L. Zhang, T. Dai, Z. Qin, H. Lu, L. Zhang, and F. Zhou, Signal Transduction Targeted Ther. **6**, 290 (2021).
[40]A. A. Hyman, C. A. Weber, and F. Jülicher, Annu. Rev. Cell Dev. Biol. **30**, 39 (2014).
[41]A. Ianiro, H. Wu, M. M. J. van Rijt, M. P. Vena, A. D. A. Keizer, A. C. C. Esteves, R. Tuinier, H. Friedrich, N. A. J. M. Sommerdijk, and J. P. Patterson, Nat. Chem. **11**, 320 (2019).
[42]Å. A. Skjevik, B. D. Madej, C. J. Dickson, C. Lin, K. Teigen, R. C. Walker, and I. R. Gould, Phys. Chem. Chem. Phys. **18**, 10573 (2016).
[43]R. Goetz and R. Lipowsky, J. Chem. Phys. **108**, 7397 (1998).
[44]J. C. Shelley, M. Y. Shelley, R. C. Reeder, S. Bandyopadhyay, P. B. Moore, and M. L. Klein, J. Phys. Chem. B **105**, 9785 (2001).
[45]R. D. Groot and K. L. Rabone, Biophys. J. **81**, 725 (2001).
[46]M. Venturoli and B. Smit, PhysChemComm **2**, 45 (1999).
[47]I. R. Cooke and M. Deserno, J. Chem. Phys. **123**, 224710 (2005).
[48]C. Arnarez, J. J. Uusitalo, M. F. Masman, H. I. Ingólfsson, D. H. de Jong, M. N. Melo, X. Periole, A. H. De Vries, and S. J. Marrink, J. Chem. Theory Comput. **11**, 260 (2015).
[49]S. J. Marrink, H. J. Risselada, S. Yefimov, D. P. Tieleman, and A. H. de Vries, J. Phys. Chem. B **111**, 7812 (2007).
[50]M. Orsi and J. W. Essex, PLoS One **6**, e28637 (2011).
[51]E. R. May, D. I. Kopelevich, and A. Narang, Biophys. J. **94**, 878 (2008).
[52]O. Farago, J. Chem. Phys. **119**, 596 (2003).
[53]K. Satoh, S. Mita, and S. Kondo, Chem. Phys. Lett. **255**, 99 (1996).
[54]J. G. Gay and B. J. Berne, J. Chem. Phys. **74**, 3316 (1981).
[55]G. R. Luckhurst and P. S. J. Simmonds, Mol. Phys. **80**, 233 (1993).
[56]E. de Miguel, L. F. Rull, M. K. Chalam, K. E. Gubbins, and F. Van Swol, Mol. Phys. **72**, 593 (1991).
[57]E. de Miguel, L. F. Rull, M. K. Chalam, and K. E. Gubbins, Mol. Phys. **74**, 405 (1991).
[58]G. R. Luckhurst, R. A. Stephens, and R. W. Phippen, Liq. Cryst. **8**, 451 (1990).
[59]Y. Huang, W. Wang, J. K. Whitmer, and R. Zhang, Soft Matter **19**, 483 (2023).
[60]G. R. Luckhurst and K. Satoh, J. Chem. Phys. **132**, 184903 (2010).
[61]Z. Q. Chen, Y. W. Sun, X. J. Zhang, Y. L. Zhu, Z. W. Li, and Z. Y. Sun, J. Chem. Phys. **158**, 104902 (2023).
[62]E. Velasco, A. M. Somoza, and L. Mederos, J. Chem. Phys. **102**, 8107 (1995).
[63]E. Velasco and L. Mederos, J. Chem. Phys. **109**, 2361 (1998).
[64]R. C. Singh, J. Ram, and Y. Singh, Phys. Rev. E **65**, 031711 (2002).
[65]P. Mishra, J. Ram, and Y. Singh, J. Phys.: Condens. Matter **16**, 1695 (2004).
[66]G. Ayton, S. G. Bardenhagen, P. McMurtry, D. Sulsky, and G. A. Voth, J. Chem. Phys. **114**, 6913 (2001).
[67]L. Whitehead, C. M. Edge, and J. W. Essex, J. Comput. Chem. **22**, 1622 (2001).
[68]X. Sun and J. D. Gezelter, J. Phys. Chem. B **112**, 1968 (2008).
[69]C. G. Gray and K. E. Gubbins, *Theory of Molecular Fluids* (Clarendon Press, Oxford, 1984), Vol. I.
[70]J. P. Hansen and I. R. McDonald, *Theory of Simple Liquids*, 4th ed. (Academic Press, Oxford, 2013).
[71]C. Caccamo, Phys. Rep. **274**, 1 (1996).
[72]G. Pellicane, L. L. Lee, and C. Caccamo, Fluid Phase Equilib. **521**, 112665 (2020).
[73]S. A. Ansary, S. Dwivedi, and P. Mishra, J. Mol. Liq. **380**, 121795 (2023).
[74]N. Metropolis, A. W. Rosenbluth, M. N. Rosenbluth, A. H. Teller, and E. Teller, J. Chem. Phys. **21**, 1087 (1953).
[75]P. Mishra and J. Ram, Eur. Phys. J. E **17**, 345 (2005).
[76]S. Dwivedi, P. Mishra, R. C. Singh, and J. Ram, J. Mol. Liq. **222**, 1139 (2016).
[77]S. Dwivedi, P. Mishra, and J. Ram, Liq. Cryst. **43**, 195 (2016).
[78]M. Dennison, A. J. Masters, D. L. Cheung, and M. P. Allen, Mol. Phys. **107**, 375 (2009).
[79]Y. Singh, Phys. Rep. **207**, 351 (1991).
[80]T. V. Ramakrishnan and M. Yussouff, Phys. Rev. B **19**, 2775 (1979).
[81]K. Thirumoorthy, N. Nandi, and D. Vollhardt, Langmuir **23**, 6991 (2007).
[82]M. Houssa, L. F. Rull, and S. C. McGrother, J. Chem. Phys. **109**, 9529 (1998).
[83]W. Józefowicz and L. Longa, Phys. Rev. E **76**, 011701 (2007).
[84]S. Varga, I. Szalai, J. Liszi, and G. Jackson, J. Chem. Phys. **116**, 9107 (2002).
[85]A. Velikonja, S. Perutkova, E. Gongadze, P. Kramar, A. Polak, A. Macek-Lebar, and A. Iglic, Int. J. Mol. Sci. **14**, 2486 (2013).
[86]See http://lammps.sandia.gov for information about the LAMMPS molecular dynamics program.
[87]J. Kolafa and J. W. Perram, Mol. Simul. **9**, 351 (1992).
[88]P. D. Godfrin, R. Castañeda-Priego, Y. Liu, and N. Wagner, J. Chem. Phys. **139**, 154904 (2013).
[89]P. D. Godfrin, N. E. Valadez-Peres, R. Castañeda-Priego, N. Wagner, and Y. Liu, Soft Matter **10**, 5061 (2014).
[90]P. Mishra and Y. Singh, Phys. Rev. Lett. **97**, 177801 (2006).
[91]J. Ram and Y. Singh, Phys. Rev. A **44**, 3718 (1991).